Complete set of polarization transfer observables for the ^{16}O($\vec{p},\vec{n}$)^{16}F reaction at 296 MeV and 0 degrees

T. Wakasa,[1,*] M. Okamoto,[1] M. Takaki,[2] M. Dozono,[2] K. Hatanaka,[3] M. Ichimura,[4] T. Noro,[1] H. Okamura,[3,†] and Y. Sakemi[5]

[1]*Department of Physics, Kyushu University, Higashi, Fukuoka 812-8581, Japan*

[2]*Center for Nuclear Study, The University of Tokyo, Bunkyo, Tokyo 113-0033, Japan*

[3]*Research Center for Nuclear Physics, Osaka University, Ibaraki, Osaka 567-0047, Japan*

[4]*RIKEN Nishina Center for Accelerator-Based Science, The Institute of Physical and Chemical Research, Wako, Saitama 351-0198, Japan*

[5]*Cyclotron and Radioisotope Center, Tohoku University, Sendai, Miyagi 980-8578, Japan*

(Received 12 May 2011; published 27 July 2011)

We report measurements of the cross section and a complete set of polarization transfer observables for the ^{16}O($\vec{p},\vec{n}$)^{16}F reaction at a bombarding energy of $T_p = 296$ MeV and a reaction angle of $\theta_{\rm lab} = 0^\circ$. The data are compared with distorted-wave impulse approximation calculations employing the large configuration-space shell-model (SM) wave functions. The well-known Gamow-Teller and spin-dipole (SD) states at excitation energies of $E_x \lesssim 8$ MeV have been reasonably reproduced by the calculations except for the spin-parity $J^\pi = 2^-$ state at $E_x = 5.86$ MeV. The SD resonance at $E_x \simeq 9.5$ MeV appears to have more $J^\pi = 2^-$ strength than $J^\pi = 1^-$ strength, consistent with the calculations. The data show significant strength in the spin-longitudinal polarized cross section $I D_L(0^\circ)$ at $E_x \simeq 15$ MeV, which indicates the existence of the $J^\pi = 0^-$ SD resonance as predicted in the SM calculations.

DOI: 10.1103/PhysRevC.84.014614 PACS number(s): 25.40.Kv, 24.70.+s, 25.10.+s

I. INTRODUCTION

The details of spin excitations in nuclei remain interesting and stimulating problems in a variety of aspects [1]. In particular, quenching of the Gamow-Teller (GT) ($L = 0$, $S = 1$, $J^\pi = 1^+$) strength in nuclei has been the subject of intensive theoretical and experimental investigation [2]. The (p,n) and (n,p) reactions in the intermediate energy region have been found to be extremely useful probes for studying the spin-isospin $\boldsymbol{\sigma\tau}$ correlations in nuclei with refined accuracy. Recent experimental studies [3,4] have revealed that GT quenching is mainly caused by coupling to two-particle–two-hole ($2p$-$2h$) excitations, while the Δ-hole coupling plays a minor role.

Spin-dipole (SD) ($L = 1$, $S = 1$, and $J^\pi = 0^-, 1^-$, and 2^-) excitations have also been studied extensively in experimental studies. Theoretical investigations of SD excitations give rise to interesting problems, especially in relation to nuclear structure [5–7] and astrophysical considerations [8]. In the $A = 12$ system, the SD resonances (SDRs) were found to occur at excitation energies of $E_x \simeq 4$ and 7 MeV. The former SDR is assigned as $J^\pi = 2^-$ [9] while the latter SDR is considered to be mainly $J^\pi = 1^-$ from the studies of the cross sections for the ^{12}C$(p,n)^{12}$N [10,11] and ^{12}C$(n,p)^{12}$B [12,13] reactions. The $J^\pi = 1^-$ dominance for the SDR at $E_x \simeq$ 7 MeV has been supported by measurements of both the proton decay of the SDR in ^{12}N populated by the ^{12}C(^{3}He, t)^{12}N reaction at ^{3}He incident energies of $T_{^3\rm He} = 75$ and 81 MeV [14] and the neutron decay of the SDR in ^{12}B populated by the ^{12}C$(d,^2$He$)^{12}$B reaction at a deuteron incident energy of $T_d = 200$ MeV [15]. However, measurement of the tensor analyzing power for the ^{12}C$(\vec{d},^2$He$)^{12}$B reaction at $T_d = 270$ MeV suggests that the SDR mainly consists of $J^\pi = 2^-$ [16]. This result has been supported by measurement of the complete set of polarization observables for the ^{12}C$(\vec{p},\vec{n})^{12}$N reaction at a proton incident energy of $T_p = 296$ MeV and a reaction angle of $\theta_{\rm lab} = 0^\circ$ [17]. The later high-resolution measurement for the ^{12}C$(\vec{d},^2$He$)^{12}$B reaction at $T_d = 171$ MeV [18] reveals that the low- and high-energy parts of the SDR at $E_x \simeq 7$ MeV mainly consist of $J^\pi = 2^-$ and 1^- strengths, respectively. Similar conclusions are made by Inomata *et al.* [15] from measurement of the proton decay of the SDR in ^{12}N produced by the ^{12}C$(^3$He$,t)^{12}$N reaction at $T_{^3\rm He} =$ 450 MeV. They also conclude that the high-energy part of the SDR at $E_x \simeq 4$ MeV in ^{12}N mainly consists of $J^\pi = 1^-$ by the same measurement, suggesting the fragmentation of the $J^\pi = 1^-$ strength. This fragmentation has been supported by theoretical calculations including the tensor correlation [19] and the deformation effect [20].

Another long-standing problem in relation to SD excitations in such systems is the missing $J^\pi = 0^-$ strength. In the $A = 12$ system, shell-model (SM) calculations predict a fairly large $J^\pi = 0^-$ SD state at $E_x \simeq$ 8–9 MeV. Extensive experimental efforts have been made to identify this $J^\pi = 0^-$ state by measuring the cross section; however, clear evidence was not obtained. Recently, the tensor analyzing powers in the $(\vec{d},^2$He) reaction [18,21] and the polarization transfer observables in the $(\vec{p},\vec{n})$ reaction [17] have been measured. The results of these measurements suggest the existence of $J^\pi = 0^-$ states at $E_x = 9.3$ and 8.4 MeV in ^{12}B and ^{12}N, respectively.

For the $A =$16 system, the $J^\pi = 0^-$ and 1^- SD strengths were also found to be missing in a study of the tensor analyzing powers for the ^{16}O$(\vec{d},^2$He$)^{16}$N reaction at $T_d =$ 270 MeV [22]. Evidence for the missing 0^- state predicted by the SM calculations was suggested in a study of the

*wakasa@phys.kyushu-u.ac.jp;http://ne.phys.kyushu-u.ac.jp/wakasa

†Deceased.

^{16}O($\vec{p}$,$\vec{n}$)^{16}F reaction at $T_p = 135$ MeV [23]; however, this has not been settled. It should be noted that the SD excitations in ^{16}O have been discussed in relation to neutrino detection from supernovae at the Super-Kamiokande water Cherenkov detector [8]. Thus, it is very important to obtain quantitative information on the distribution of the SD strengths in such systems.

In this article, we present the double-differential cross section and a complete set of polarization transfer observables for the ^{16}O($\vec{p}$,$\vec{n}$)^{16}F reaction at $T_p = 296$ MeV and $\theta_{\rm lab} = 0^\circ$. It should be noted that the SD states are fairly strongly excited even at $\theta_{\rm lab} = 0^\circ$ [23] because the GT transitions are largely inhibited for a double LS closed shell nucleus as occurs in ^{16}O. In addition, distortion effects are minimal at $T_p \simeq 300$ MeV [2], thereby enabling the extraction of reliable nuclear structure information on the SDRs. Polarization transfer observables are sensitive to the spin-parity of an excited state [24], as was demonstrated for the SDR in ^{12}N [17]. They are used to separate the cross section into nonspin $ID_0(0^\circ)$, spin-longitudinal $ID_L(0^\circ)$, and spin-transverse $ID_T(0^\circ)$ polarized cross sections. The observed $ID_i(0^\circ)$ are compared with distorted-wave impulse approximation (DWIA) calculations employing the large configuration-space SM wave functions [25] in order to access the spin-isospin excitations in ^{16}F, e.g., the missing $J^\pi = 0^-$ and 1^- SD strengths.

II. EXPERIMENTAL METHODS

Measurements were performed with a neutron time-of-flight (NTOF) system [26] and a neutron detector and polarimeter (NPOL3) [27] at the Research Center for Nuclear Physics (RCNP) at Osaka University. Detailed descriptions of the NTOF and NPOL3 systems are found in Refs. [26,27]. Thus, in the following, we only describe the detector system briefly and discuss experimental details relevant to the present experiments.

A. Polarized proton beam

The polarized proton beam from the high-intensity polarized ion source (HIPIS) at RCNP [28] was accelerated up to $T_p = 53$ and 296 MeV by using the AVF and Ring cyclotrons, respectively. The beam polarization direction was reversed every 5 s by selecting rf transitions in order to minimize geometrical false asymmetries. For the cross section measurements, one out of seven beam pulses was selected for injection into the Ring cyclotron, which then yielded a beam pulse period of 453 ns. This pulse selection reduces the wraparound of slow neutrons from preceding beam pulses. For the polarization transfer measurements, pulse selection was not performed in order to achieve reasonable statistical accuracy. In both measurements, single-turn extraction from the Ring cyclotron was used in order to maintain the beam polarization.

The superconducting solenoid magnets, SOL1 and SOL2 [26], were located in the injection line from the AVF to the Ring cyclotrons to precess the proton spin direction. Each magnet can rotate the direction of the polarization vector from the normal $\hat{N}$ into the sideways $\hat{S}$ directions. The two magnets were installed in front of (SOL1) and behind (SOL2) the 45° bending magnet, and the spin precession angle in this bending magnet was about 85.2° for $T_p = 53$ MeV protons. Therefore, we can obtain proton beams with longitudinal ($\hat{L}$) and sideways ($\hat{S}$) polarizations at the exit of the SOL2 by using the SOL1 and SOL2 magnets, respectively.

The beam polarization was continuously monitored by two sets of beam-line polarimeters, BLP1 and BLP2 [26], which were installed in front of and behind the 98° bending magnet, respectively. Each polarimeter consists of four conjugate-angle pairs of plastic scintillators, and determines the beam polarization via the $\vec{p} + p$ elastic scattering in the $\hat{N}$ and $\hat{S}$ directions. A self-supporting polyethylene (CH_2) target with an areal density of 1.1 mg/cm^2 was used as the hydrogen target, and the elastically scattered and recoiled protons were detected in kinematical coincidence with a pair of scintillators. The spin precession angle in the 98° bending magnet was about 231.1° for $T_p = 296$ MeV protons. Therefore, all components (p_S, p_N, p_L) of the polarization vector can be simultaneously determined using BLP1 and BLP2. The typical magnitude of the beam polarization was about 0.62.

B. ^{16}O target

The ^{16}O target was prepared as a windowless and self-supporting ice (H_2O) target [29]. This target was operated at temperatures down to 77 K by using liquid nitrogen, and the typical areal density was about 147 mg/cm^2. The thickness was determined by comparing the ^{16}O(p,n)^{16}F yield to that from a SiO_2 target with an areal density of 221 mg/cm^2. Since the hydrogen does not produce any physical background in the present energy region, we have successfully obtained very clean spectra for the ^{16}O(p,n)^{16}F reaction.

C. Neutron spin-rotation magnet and NPOL3

A dipole magnet for neutron spin-rotation (NSR magnet) was positioned at the entrance of the time-of-flight (TOF) tunnel. This magnet was used to precess the neutron polarization vector from the longitudinal direction, $\hat{L}'$, to the normal direction, $\hat{N}'$, so as to allow the longitudinal component to be measured with NPOL3 as the normal component.

Neutrons were measured by the NPOL3 system [27] with a 100-m-flight-path length. The NPOL3 system consists of three planes of neutron detectors. Each of the first two planes (HD1 and HD2) consists of 10 sets of one-dimensional position-sensitive plastic scintillators (BC408) with a size of 100 × 10 × 5 cm^3. Each plane has an effective detection area of 1 m^2. The last plane (NC) is a two-dimensional position-sensitive plastic scintillator with a size of 100 × 100 × 10 cm^3. Both HD1 and HD2 planes serve as neutron detectors and neutron polarization analyzers for the cross section and polarization transfer measurements, respectively, and the NC plane acts as a catcher for the particles scattered by the HD1 or HD2 plane.

III. DATA REDUCTION

A. Neutron detection efficiency

The neutron detection efficiency of NPOL3 (HD1 and HD2) was determined using the ^{12}C$(p,n)^{12}$N(g.s., 1^+) reaction at $\theta_{\rm lab} = 0^\circ$, which has a known cross section at $T_p = 296$ MeV [30,31]. The result was 0.048 ± 0.003 with the overall uncertainty mainly coming from uncertainties in the cross section and thickness of the ^{12}C target.

B. Effective analyzing power

The neutron polarization was analyzed by monitoring $\vec{n} + p$ scattering at either neutron detector HD1 or HD2, and the recoiled protons were detected with neutron detector NC. The effective analyzing power $A_{y;\rm eff}$ of NPOL3 was determined by using polarized neutrons from the GT transition in the ^{12}C$(p,n)^{12}$N(g.s., 1^+) reaction at $T_p = 296$ MeV and $\theta_{\rm lab} = 0^\circ$. We used two kinds of polarized protons with normal (p_N) and longitudinal (p_L) polarizations. The corresponding neutron polarizations at 0° become $p'_N = p_N D_{NN}(0^\circ)$ and $p'_L = p_L D_{LL}(0^\circ)$, respectively. The resulting asymmetries measured by NPOL3 are

$$\epsilon_N = p'_N A_{y;\rm eff} = p_N D_{NN}(0^\circ) A_{y;\rm eff}, \tag{1a}$$

$$\epsilon_L = p'_L A_{y;\rm eff} = p_L D_{LL}(0^\circ) A_{y;\rm eff}. \tag{1b}$$

Because the polarization transfer observables for the GT transition satisfy [32]

$$2D_{NN}(0^\circ) + D_{LL}(0^\circ) = -1, \tag{2}$$

$A_{y;\rm eff}$ can be expressed in terms of Eqs. (1) and (2) as

$$A_{y;\rm eff} = -\left(2\frac{\epsilon_N}{p_N} + \frac{\epsilon_L}{p_L}\right). \tag{3}$$

Therefore, the $A_{y;\rm eff}$ value can be obtained without knowing a priori the values of $D_{ii}(0^\circ)$, giving a result of $A_{y;\rm eff} = 0.131 \pm 0.004$, in which the uncertainty is statistical.

The $D_{NN}(0^\circ)$ value at $T_p = 296$ MeV, which is determined from Eq. (1a) using the obtained value for $A_{y;\rm eff}$, is $D_{NN}(0^\circ) = -0.216 \pm 0.013$. This value for $D_{NN}(0^\circ)$ is consistent with a previous value of $D_{NN}(0^\circ) = -0.227 \pm 0.010$ [31], demonstrating the reliability of our calibrations.

IV. RESULTS

A. Cross section and polarization transfer observables

Figure 1 shows the double-differential cross section I and the complete set of polarization transfer observables $D_{NN}(0^\circ)$ and $D_{LL}(0^\circ)$ for the ^{16}O$(\vec{p},\vec{n})^{16}$F reaction at $T_p = 296$ MeV and $\theta_{\rm lab} = 0^\circ$. The data for the cross section are binned in 0.1 MeV intervals, while the data for $D_{ii}(0^\circ)$ are binned in 0.5 MeV intervals to reduce statistical fluctuations. Excitation of the well-known GT and SD states [33] at $E_x \lesssim 8$ MeV can be seen. The peak at $E_x \simeq 0$ MeV is a sum of the $J^\pi = 0^-, 1^-$, and 2^- states, while the shoulder at $E_x = 3.76$ and the peak at $E_x = 4.65$ MeV are the $J^\pi = 1^+$ states. Both the peak at

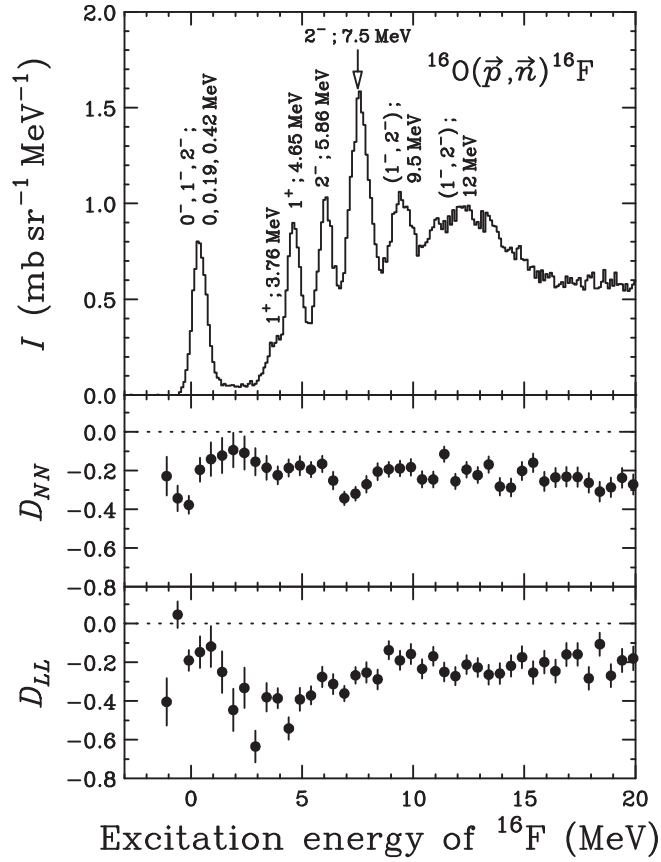

FIG. 1. Double-differential cross section spectrum I (top panel), and a complete set of polarization transfer observables $D_{NN}(0^\circ)$ (middle panel) and $D_{LL}(0^\circ)$ (bottom panel) for the ^{16}O$(\vec{p},\vec{n})^{16}$F reaction at $T_p = 296$ MeV and $\theta_{\rm lab} = 0^\circ$.

$E_x = 5.86$ and the narrow resonance at $E_x \simeq 7.5$ MeV are known as $J^\pi = 2^-$ states. The other narrow and broad resonances at $E_x \simeq 9.5$ and 12 MeV have been suggested to be features of the $J^\pi = 1^-$ and 2^- states [33].

An interesting feature of the $D_{ii}(0^\circ)$ data is that negative values are obtained over the entire excitation region. It should be noted that the $D_{NN}(0^\circ)$ value of a natural-parity transition is predicted to be positive in the plane-wave impulse approximation (PWIA) theory [24]. Thus, the observed negative $D_{NN}(0^\circ)$ values for the resonances at $E_x \simeq 9.5$ and 12 MeV indicate significant unnatural-parity contributions, such as from $J^\pi = 2^-$ and 1^+ states, which are consistent with a previous result obtained for the ^{16}O$(^3$He$,t)^{16}$F reaction at $T_{^3\rm He} = 81$ MeV [34].

B. Polarized cross sections

The double-differential cross section I can be separated into nonspin $I D_0$, spin-longitudinal $I D_q$, and two spin-transverse $I D_n$ and $I D_p$ polarized cross sections as follows:

$$I = I D_0 + I D_q + I D_n + I D_p, \tag{4}$$

where D_i are the polarization observables introduced by Bleszynski *et al.* [35]. Here, we also use the spin-longitudinal $I D_L(0^\circ)$ and spin-transverse $I D_T(0^\circ)$ polarized cross sections,

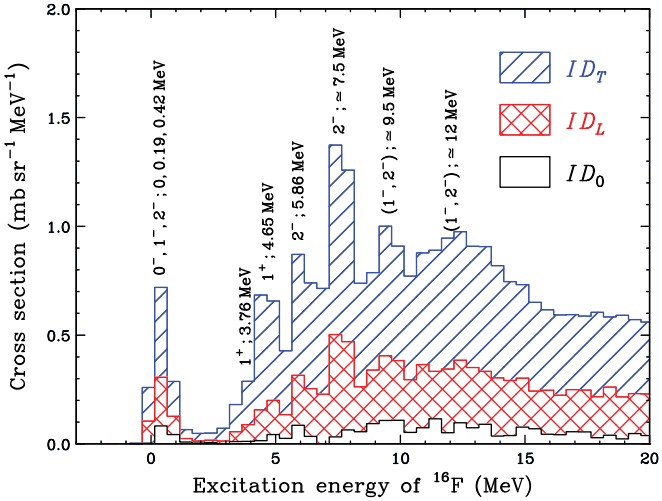

FIG. 2. (Color online) Nonspin ID_0 (unfilled), spin-longitudinal ID_L (cross hatched), and spin-transverse ID_T (hatched) polarized cross sections for the ^{16}O($\vec{p},\vec{n}$)^{16}F reaction at $T_p = 296$ MeV and $\theta_{\rm lab} = 0^\circ$.

which are defined at $\theta_{\rm lab} = 0^\circ$ as [17]

$$ID_L(0^\circ) \equiv ID_q(0^\circ) = \frac{I}{4}\left[1 - 2D_{NN}(0^\circ) + D_{LL}(0^\circ)\right], \tag{5a}$$

$$ID_T(0^\circ) \equiv ID_n(0^\circ) + ID_p(0^\circ) = \frac{I}{2}\left[1 - D_{LL}(0^\circ)\right]. \tag{5b}$$

Figure 2 shows the polarized cross sections, $ID_L(0^\circ)$, $ID_T(0^\circ)$, and $ID_0(0^\circ)$, for the ^{16}O(p,n)^{16}F reaction at $T_p = 296$ MeV and $\theta_{\rm lab} = 0^\circ$. The data are binned in 0.5 MeV intervals to reduce statistical fluctuations. The spin-longitudinal cross section $ID_L(0^\circ)$ consists exclusively of unnatural-parity transitions, such as $J^\pi = 1^+$ and 2^-, whereas the spin-transverse cross section $ID_T(0^\circ)$ consists of both the natural- and unnatural-parity transitions [24]. Note that the unnatural-parity $J^\pi = 0^-$ transition is a special case, and it contributes to $ID_L(0^\circ)$ only. The peaks and resonances at $E_x \lesssim 8$ MeV are observed for both $ID_L(0^\circ)$ and $ID_T(0^\circ)$, which are consistent with their unnatural-parity assignments to either $J^\pi = 2^-$ or 1^+ states. At $E_x \simeq 9.5$ MeV, resonances are observed for both $ID_L(0^\circ)$ and $ID_T(0^\circ)$ while at $E_x \simeq 12$ MeV only $ID_T(0^\circ)$ displays a resonance. These results suggest that the dominant components for the resonances at $E_x \simeq 9.5$ and 12 MeV are the $J^\pi = 2^-$ and 1^- states, respectively, as will be discussed in greater detail in the next section in relation to the DWIA calculations.

It is interesting to note that the sum of the $J^\pi = 0^-$, 1^-, and 2^- SD states at $E_x \simeq 0$ MeV forms a significant peak in the $ID_0(0^\circ)$ spectrum. In PWIA theory, it is considered that a SD state could not contribute to $ID_0(0^\circ)$ due to its spin-flip character. However, the $J^\pi = 1^-$ state may be apparent due to distortion effects [17]. Therefore, the $J^\pi = 1^-$ component is considered to give rise to the peak in the $ID_0(0^\circ)$ spectrum, which will also be investigated in the next section.

V. DISCUSSION

A. DWIA calculations

DWIA calculations were performed on the data using a computer code DW81 [36]. The one-body density matrix elements (OBDMEs) for the ^{16}O(p,n)^{16}F reaction were obtained from the SM calculations [25], which were performed in the $0s$-$0p$-$1s0d$-$0f1p$ configuration space by using phenomenological effective interactions. In the calculations, the ground state of ^{16}O was described as a mixture of $0\hbar\omega$ (closed shell) and $2\hbar\omega$ configurations, and up to $3\hbar\omega$ configurations were included in the final states. The $2\hbar\omega$ admixture in the ground state provides significant GT strength which is similar to that obtained by Haxton and Johnson [37], and the transition strengths for negative-parity states are uniformly reduced by a factor of about 0.7 [25]. The single particle wave functions were generated by the sum of a Woods-Saxon (WS) potential with $r_0 = 1.27$ fm, $a_0 = 0.67$ fm [38], a spin-orbit potential with $V_{ls} = 10.4$ MeV [39], and the Coulomb potential. The depth of the WS potential was adjusted to reproduce the separation energies of the $0p_{1/2}$ orbits. The unbound single particle states were assumed to have a shallow binding energy of 0.01 MeV in order to simplify the calculations. The distorted wave for the protons was generated using a global optical model potential (OMP) in the proton energy range $T_p = 20$–1040 MeV [40], while that for neutrons was generated using a global OMP in the neutron energy range $T_n = 20$–1000 MeV [41].

B. Effective NN interactions

The polarization transfer observables D_{ij} are sensitive to both the spin-parity of the excited state and the effective nucleon-nucleon (NN) interaction. Thus, in order to use the D_{ij} values for the spin-parity assignments, we have checked and modified the effective NN interaction parameterized by Franey and Love at 325 MeV [42]. For this purpose, the experimental data for well-resolved $J^\pi = 1^+$ (g.s.) and 2^- (4.14 MeV) states of the ^{12}C($\vec{p},\vec{n}$)^{12}N reaction at the same energy [30,31] were compared with the DWIA calculations. In the calculations, the OBDMEs were obtained by using a computer code NUSHELL@MSU [43] with the interaction in the $0p$-$1s0d$ configuration space of Millener and Kurath (PSDMKII) [44].

It was found that the $D_{ii}(0^\circ)$ values for the $J^\pi = 1^+$ state are reasonably reproduced by the calculations, which is consistent with previous results [30,31]. However, those for the $J^\pi = 2^-$ state could not be reproduced, e.g., the experimental value was $D_{LL}(0^\circ) = -0.36 \pm 0.09$, while the theoretical value was -0.85. It should be noted that the $D_{ii}(0^\circ)$ values are sensitive to the tensor component of the interaction [45–47]. Thus, we tried to modify the tensor component to reproduce the experimental data.

The isovector V_τ^T and isoscalar V_0^T exchange tensor interactions are described with the tensor-even $V^{\rm TNE}$ and tensor-odd $V^{\rm TNO}$ interactions as [45,48]

$$V_\tau^T = -\tfrac{1}{4}(V^{\rm TNE} + V^{\rm TNO}), \tag{6a}$$

$$V_0^T = \tfrac{1}{4}(V^{\rm TNE} - 3V^{\rm TNO}). \tag{6b}$$

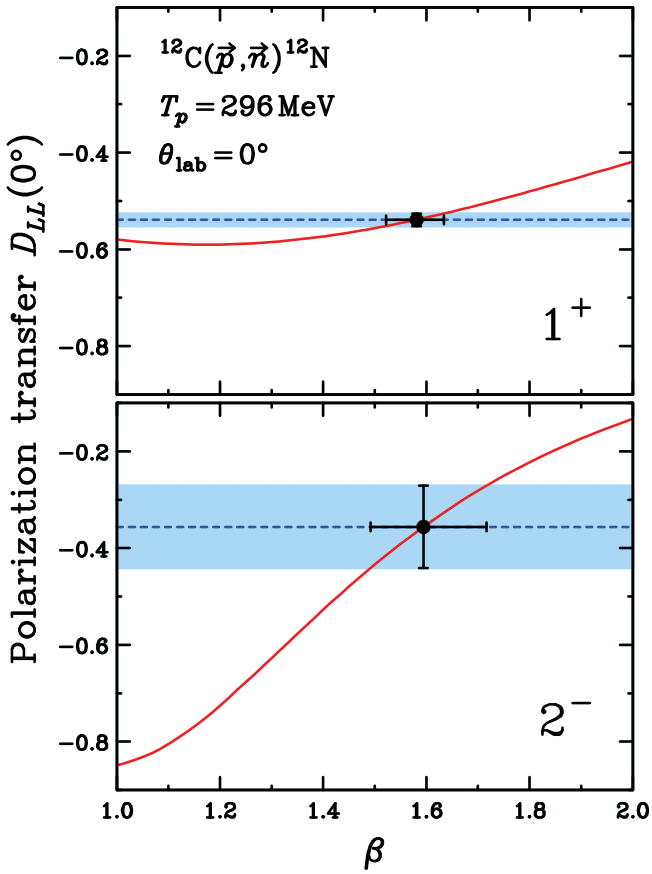

FIG. 3. (Color online) Polarization transfer $D_{LL}(0^\circ)$ for the ^{12}C($\vec{p}$,$\vec{n}$)^{12}N(g.s., 1^+) (upper panel) and ^{12}C($\vec{p}$,$\vec{n}$)^{12}N(4.2 MeV, 2^-) (lower panel) reactions at T_p = 296 MeV and $\theta_{lab} = 0^\circ$ [31]. The data are shown by the filled circles and horizontal dashed lines, and the corresponding uncertainties shown by the vertical error bars and horizontal bands. The curves represent the results of the DWIA calculations as a function of β as defined in Eq. (7). See the main text for details.

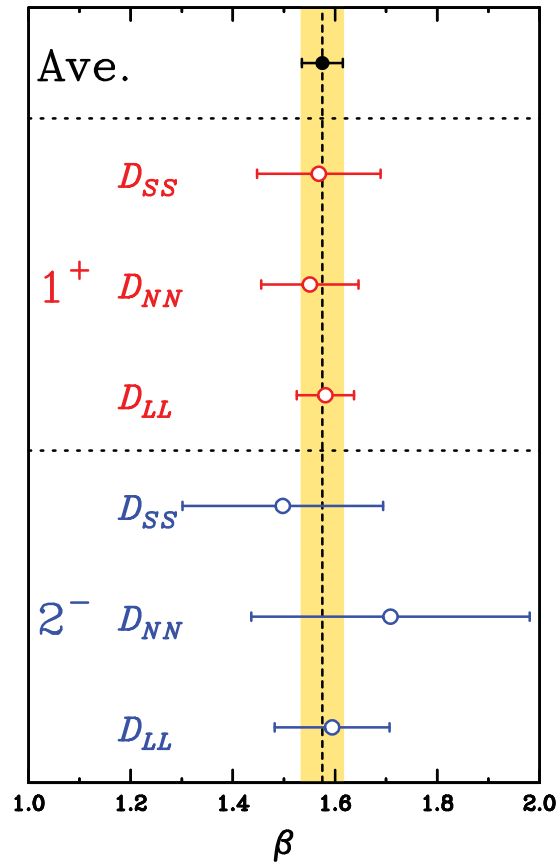

FIG. 4. (Color online) Optimization of the β values [see Eq. (7)] to reproduce the polarization transfer observables $D_{ii}(0^\circ)$ for the ^{12}C($\vec{p}$,$\vec{n}$)^{12}N(g.s., 1^+) and ^{12}C($\vec{p}$,$\vec{n}$)^{12}N(4.2 MeV, 2^-) reactions at T_p = 296 MeV and $\theta_{lab} = 0^\circ$ [31]. The vertical line and band represent the averaged value and its uncertainty, respectively.

We modified the isovector V_τ^T interaction while keeping the isoscalar V_0^T tensor interaction unchanged according to Ref. [49]. Thus, the modified tensor-even $\tilde{V}^{\rm TNE}$ and tensor-odd $\tilde{V}^{\rm TNO}$ interactions are described in relation to the parameter β as

$$\tilde{V}^{\rm TNE} = V^{\rm TNE} + 3(\beta - 1)V^{\rm TNO}, \tag{7a}$$

$$\tilde{V}^{\rm TNO} = \beta V^{\rm TNO}, \tag{7b}$$

where $\tilde{V}^{\rm TNE} = V^{\rm TNE}$ and $\tilde{V}^{\rm TNO} = V^{\rm TNO}$ for $\beta = 1$. The long-range part of the isovector tensor interaction is well known from the one-pion exchange model; however, the short-range part has not been determined as accurately. Thus, we modified only the imaginary part of the short-range $V^{\rm TNE}$ and $V^{\rm TNO}$ interactions, which have a range of 0.25 fm, because the $D_{ii}(0^\circ)$ value for the $J^\pi = 2^-$ state is sensitive to these components.

The upper and lower panels of Fig. 3 represent the $D_{LL}(0^\circ)$ values for the $J^\pi = 1^+$ and 2^- states, respectively, as a function of β. The experimental data are shown by filled circles and horizontal dashed lines, and the corresponding uncertainties shown as vertical error bars and horizontal bands. The $D_{LL}(0^\circ)$ values for both the $J^\pi = 1^+$ and 2^- states are well reproduced using $\beta \simeq 1.6$ with uncertainties of $\delta\beta \simeq 0.1$. The optimum β values were also deduced for the other polarization transfers $D_{SS}(0^\circ)$ and $D_{NN}(0^\circ)$, and the results are summarized in Fig. 4. All the $D_{ii}(0^\circ)$ data support the modification of the tensor component using $\beta \simeq 1.6$. In the following, therefore, we use the averaged value of $\beta = 1.58 \pm 0.04$ in the DWIA calculations.

C. Comparison with theoretical calculations

Figure 5 compares the experimental polarized cross sections $I\,D_i(0^\circ)$ with the theoretical calculations. The intrinsic widths Γ have been neglected for the states at $E_x < 9.5$ MeV, where narrow peaks and resonances are observed, whereas widths of $\Gamma = 2$ MeV were used for the states at $E_x \geqslant 9.5$ MeV. The results of the calculations were convoluted with a Gaussian function with an experimental resolution of 700 keV in the full-width at half-maximum (FWHM). The shaded, cross-hatched, hatched, and unfilled regions correspond to the $J^\pi = 1^+$, 0^-, 1^-, and 2^- components, respectively. The

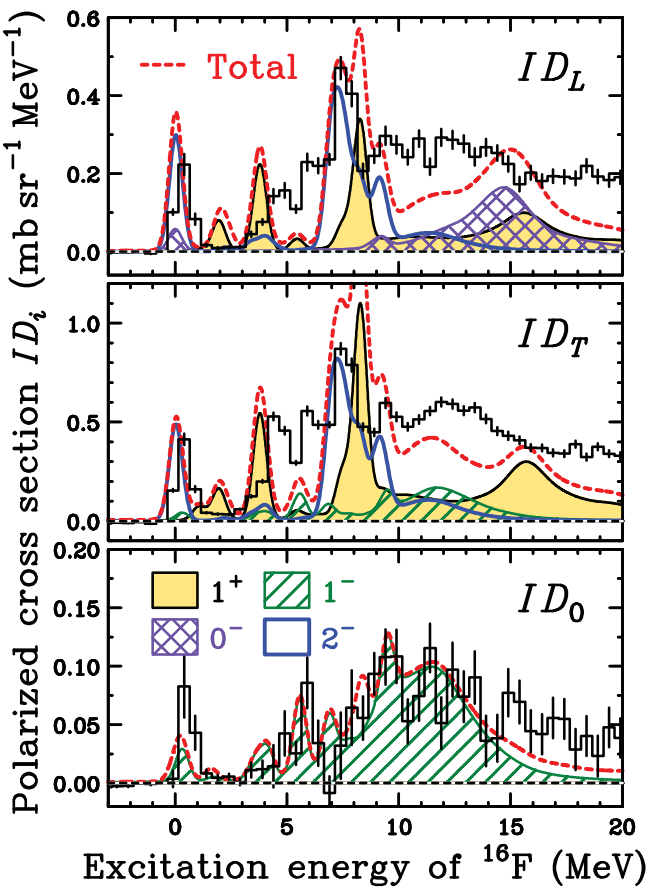

FIG. 5. (Color online) Spin-longitudinal ID_L (top panel), spin-transverse ID_T (middle panel), and nonspin ID_0 (bottom panel) polarized cross sections for the ^{16}O$(\vec{p},\vec{n})^{16}$F reaction at $T_p = 296$ MeV and $\theta_{\rm lab} = 0^\circ$. The shaded, cross-hatched, hatched, and unfilled regions represent the results of the DWIA calculations for the $J^\pi = 1^+$, 0^-, 1^-, and 2^- components, respectively. The dashed curves show the total ID_i including contributions of up to $J^\pi = 4^-$. The intrinsic widths for the states at $E_x \geqslant 9.5$ MeV have been set to $\Gamma = 2$ MeV. The DWIA results have been convoluted with a Gaussian function with an experimental energy resolution of 700 keV in FWHM.

total $ID_i(0^\circ)$ spectrum, including components up to $J^\pi = 4^-$, are shown by the dashed curves, although the contributions from $L = 2$–4 components are small. As expected in a simple PWIA [24], the spin-longitudinal cross section $ID_L(0^\circ)$ consists exclusively of the unnatural-parity $J^\pi = 1^+$, 0^-, and 2^- transitions, whereas the spin-transverse cross section $ID_T(0^\circ)$ consists of the unnatural-parity $J^\pi = 1^+$ and 2^- transitions as well as the natural-parity $J^\pi = 1^-$ transition. Note that the natural-parity $J^\pi = 1^-$ transition is predominant in the spin-scalar cross section $ID_0(0^\circ)$.

The peaks at $E_x \simeq 0$ MeV in the $ID_L(0^\circ)$ and $ID_T(0^\circ)$ spectra are reasonably reproduced as a combination of the dominant $J^\pi = 2^-$ contribution with weak $J^\pi = 0^-$ and 1^- contributions. The $J^\pi = 2^-$ state at $E_x \simeq 7.5$ MeV is also well reproduced in the present calculations. Furthermore, the SDR at $E_x \simeq 9.5$ MeV observed in both the $ID_L(0^\circ)$ and $ID_T(0^\circ)$ spectra is reasonably reproduced by the calculations as the $J^\pi = 2^-$ state. Thus, we conclude that the SDR at $E_x \simeq 9.5$ MeV is dominated by the $J^\pi = 2^-$ state.

It is interesting that the $J^\pi = 2^-$ state at $E_x = 5.86$ MeV could not be reproduced. In the SM calculations, the $(0p^{-1}_{1/2}0d_{5/2})$, $(0p^{-1}_{1/2}0d_{3/2})$, $(0p^{-1}_{3/2}0d_{5/2})$, and $(0p^{-1}_{3/2}0d_{3/2})$ configurations are dominant for the experimental $J^\pi = 2^-$ states at $E_x = 0.42$, 5.86, $\simeq$7.5, and $\simeq$9.5 MeV, respectively. It should be noted that the $J^\pi = 2^-$ state at $E_x = 5.86$ MeV is predicted to have a significant contribution from the $(0p^{-1}_{3/2}1s_{1/2})$ configuration. The interference between $(0p^{-1}_{1/2}0d_{3/2})$ and $(0p^{-1}_{3/2}1s_{1/2})$ reduces the transition strength, and thus the $ID_i(0^\circ)$ becomes very small. This quenching is also exhibited in a standard SM calculation [19] using the PSDMKII interaction [44]. Thus, further detailed theoretical investigations are definitely required to resolve the discrepancy for the $J^\pi = 2^-$ state at $E_x = 5.86$ MeV.

For the $J^\pi = 1^+$ GT transitions, the calculations provide reasonable predictions of the magnitudes of the peaks at $E_x = 3.76$ and 4.65 MeV in both the $ID_L(0^\circ)$ and $ID_T(0^\circ)$ spectra, even though the excitation energies are significantly lower at $E_x \simeq 1.9$ and 3.8 MeV. The calculations also predict concentrations at $E_x \simeq 8.3$ and 15.7 MeV, which are inconsistent with the experimental data. A possible explanation for these features is that the strengths are fragmented by enlarging the

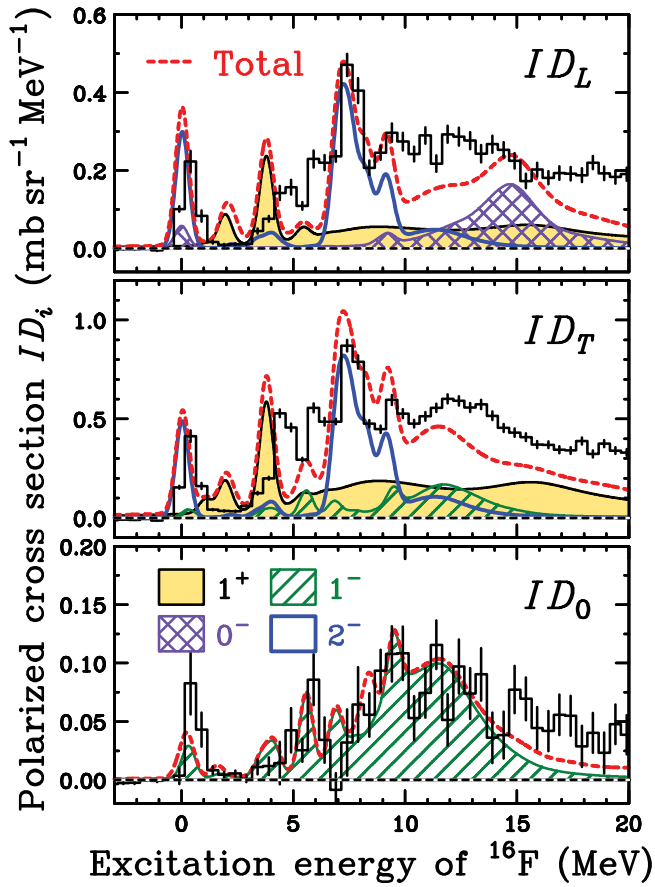

FIG. 6. (Color online) Same as Fig. 5 but the intrinsic widths for the GT 1^+ states at $E_x \geqslant 7$ MeV have been set to $\Gamma = 5$ MeV. See text for details.

configuration space. Figure 6 shows the results of calculations with $\Gamma = 5$ MeV for the GT states at $E_x \geqslant 7$ MeV, which provides a better description of both $I D_L(0^\circ)$ and $I D_T(0^\circ)$ values. The present data support the significant GT strengths predicted in the SM calculations. However, the calculations underestimate both $I D_L(0^\circ)$ and $I D_T(0^\circ)$ at $E_x \gtrsim 10$ MeV. This underestimation might be resolved by considering the $4\hbar\omega$ configurations [37].

For the $J^\pi = 1^-$ SD transitions, two peaks which correspond to the states at $E_x = 0.19$ and 5.24 MeV are clearly observed in the $I D_0(0^\circ)$ spectrum. The observed state at $E_x = 5.24$ MeV in $I D_0(0^\circ)$ supports a tentative spin-parity assignment of the $J^\pi = 1^-$ state [33]. The $I D_0(0^\circ)$ peak for the state at $E_x = 5.24$ MeV is well reproduced by the theoretical calculations, whereas that at $E_x = 0.19$ MeV is underestimated, although the experimental uncertainty is large. The broad bumps in $I D_0(0^\circ)$ and $I D_T(0^\circ)$ at $E_x \simeq 12$ MeV are reasonably reproduced as the giant dipole resonance (GDR) and SDR, respectively. It should be noted that this broad bump is not observed in either the experimental or theoretical $I D_L(0^\circ)$ spectrum, and thus it is natural to conclude that the bump is dominated by both 1^- SDR and GDR.

Concerning the $J^\pi = 0^-$ SD transitions, the theoretical calculations predict both the well-established state at $E_x = 0$ MeV and the missing SDR at $E_x \simeq 15$ MeV. The significant strength observed in $I D_L(0^\circ)$ at around $E_x = 15$ MeV supports the existence of the $J^\pi = 0^-$ SDR in this region. However, the experimental data does not show a clear bump in this region, and thus the $J^\pi = 0^-$ strengths are likely to be more fragmented. Therefore, further detailed theoretical investigations are also required to determine the distribution of the $J^\pi = 0^-$ SDR.

VI. SUMMARY AND CONCLUSION

The cross section and a complete set of polarization transfer observables were measured for the ^{16}O$(\vec{p},\vec{n})^{16}$F reaction at $T_p = 296$ MeV and $\theta_{\rm lab} = 0^\circ$. The experimental polarized cross sections $I D_i(0^\circ)$ ($i = 0$, L, and T) were compared with DWIA calculations, employing SM wave functions of up to $3\hbar\omega$ configurations. The GT and SD states at $E_x \lesssim 8$ MeV have been reasonably reproduced by the DWIA calculations, with the exception of the $J^\pi = 2^-$ state at $E_x = 5.86$ MeV, in which the predicted contribution from the $(0p_{3/2}^{-1}1s_{1/2})$ configuration seems to be inappropriate. The SDR at $E_x \simeq 9.5$ MeV appears to have more $J^\pi = 2^-$ strength than $J^\pi = 1^-$ strength at $\theta_{\rm lab} = 0^\circ$, whereas the bump at $E_x \simeq 12$ MeV is reasonably explained as the sum of the $J^\pi = 1^-$ GDR and SDR. The data show a significant strength in $I D_L(0^\circ)$ at $E_x \simeq 15$ MeV, which can be attributed to the $J^\pi = 0^-$ SDR predicted in the SM calculations. These findings, and further studies applying polarization transfer measurements to other nuclei, will provide valuable insight for studies into nuclear structure, e.g., tensor correlations in nuclear spin excitations.

ACKNOWLEDGMENTS

We are grateful to Professor T. Kawabata for his helpful correspondence. We also acknowledge the dedicated efforts of the RCNP cyclotron crew for providing a high-quality polarized proton beam. The experiment was performed at RCNP under Program No. E317. This research was supported in part by the Ministry of Education, Culture, Sports, Science, and Technology of Japan.

[1] M. N. Harakeh and A. van der Woude, *Giant Resonances: Fundamental High-Frequency Modes of Nuclear Excitation* (Oxford University Press, Oxford, 2001).
[2] M. Ichimura, H. Sakai, and T. Wakasa, Prog. Part. Nucl. Phys. **56**, 446 (2006).
[3] T. Wakasa *et al.*, Phys. Rev. C **55**, 2909 (1997).
[4] K. Yako *et al.*, Phys. Lett. B **615**, 193 (2005).
[5] N. Auerbach and A. Klein, Phys. Rev. C **30**, 1032 (1984).
[6] H. Sagawa and B. Castel, Nucl. Phys. A **435**, 1 (1985).
[7] T. Suzuki, H. Sagawa, and N. VanGiai, Phys. Rev. C **57**, 139 (1998).
[8] K. Langanke, P. Vogel, and E. Kolbe, Phys. Rev. Lett. **76**, 2629 (1996).
[9] F. Ajzenberg-Selove, Nucl. Phys. A **506**, 1 (1990).
[10] X. Yang *et al.*, Phys. Rev. C **52**, 2535 (1995).
[11] B. D. Anderson, L. A. C. Garcia, D. J. Millener, D. M. Manley, A. R. Baldwin, A. Fazely, R. Madey, N. Tamimi, J. W. Watson, and C. C. Foster, Phys. Rev. C **54**, 237 (1996).
[12] N. Olsson *et al.*, Nucl. Phys. A **559**, 368 (1993).
[13] X. Yang *et al.*, Phys. Rev. C **48**, 1158 (1993).
[14] W. A. Sterrenburg, M. N. Harakeh, S. Y. van der Werf, and A. van der Woude, Nucl. Phys. A **405**, 109 (1983).
[15] T. Inomata *et al.*, Phys. Rev. C **57**, 3153 (1998).
[16] H. Okamura *et al.*, Phys. Lett. B **345**, 1 (1995).
[17] M. Dozono *et al.*, J. Phys. Soc. Jpn. **77**, 014201 (2008).
[18] M. A. de Huu *et al.*, Phys. Lett. B **649**, 35 (2007).
[19] T. Suzuki and H. Sagawa, Nucl. Phys. A **637**, 547 (1998).
[20] H. Kurasawa and T. Suzuki, in *Proceedings of the International Symposium on New Facet of Spin Giant Resonances in Nuclei, Tokyo, Japan*, 1997, edited by H. Sakai, H. Okamura, and T. Wakasa (World Scientific, Singapore, 1998), p. 183.
[21] H. Okamura, T. Uesaka, K. Suda, H. Kumasaka, R. Suzuki, A. Tamii, N. Sakamoto, and H. Sakai, Phys. Rev. C **66**, 054602 (2002).
[22] K. Suda *et al.*, in *Proceedings of the 16th International Spin Physics Symposium, Trieste, Italy,* 2004, edited by F. Bradamante, A. Bressan, and A. Martin (World Scientific, Singapore, 2005), p. 649
[23] J. W. Watson, B. D. Anderson, A. R. Baldwin, C. C. Foster, L. Lamm, R. Madey, M. R. Plumley, and P. J. Pella, Nucl. Phys. A **577**, 79c (1994).
[24] J. M. Moss, Phys. Rev. C **26**, 727 (1982).
[25] N. Auerbach and B. A. Brown, Phys. Rev. C **65**, 024322 (2002).
[26] H. Sakai *et al.*, Nucl. Instrum. Methods Phys. Res., Sect. A **369**, 120 (1996).
[27] T. Wakasa *et al.*, Nucl. Instrum. Methods Phys. Res., Sect. A **547**, 569 (2005).
[28] K. Hatanaka *et al.*, Nucl. Instrum. Methods Phys. Res., Sect. A **384**, 575 (1997).

[29] T. Kawabata *et al*., Nucl. Instrum. Methods Phys. Res., Sect. A **459**, 171 (2001).
[30] T. Wakasa *et al*., Phys. Lett. B **656**, 38 (2007).
[31] M. Dozono *et al*., Phys. Rev. C **80**, 024319 (2009).
[32] T. Wakasa *et al*., J. Phys. Soc. Jpn. **73**, 1611 (2004).
[33] D. R. Tilley, H. R. Weller, and C. M. Cheves, Nucl. Phys. A **564**, 1 (1993).
[34] W. A. Sterrenburg *et al*., Nucl. Phys. A **420**, 257 (1984).
[35] E. Bleszynski, M. Bleszynski, and C. A. Whitten, Phys. Rev. C **26**, 2063 (1982).
[36] R. Schaeffer and J. Raynal, program DW70 (unpublished); J. Raynal, Nucl. Phys. A **97**, 572 (1967); J. R. Comfort, extended version DW81 (unpublished).
[37] W. C. Haxton and C. Johnson, Phys. Rev. Lett. **65**, 1325 (1990).
[38] A. Bohr and B. R. Mottelson, *Nuclear Structure Volume I: Single-Particle Motion* (Benjamin, New York, 1969).
[39] K. Nishida and M. Ichimura, Phys. Rev. C **51**, 269 (1995).
[40] E. D. Cooper *et al*., Phys. Rev. C **47**, 297 (1993).
[41] Shen Qing-biao, Feng Da chun, and Zhuo Yi-zhong, Phys. Rev. C **43**, 2773 (1991).
[42] M. A. Franey and W. G. Love, Phys. Rev. C **31**, 488 (1985).
[43] B. A. Brown and W. D. M. Rae, shell-model code NUSHELL@MSU, MSU-NSCL report (2007).
[44] D. J. Millener and D. Kurath, Nucl. Phys. A **255**, 315 (1975).
[45] T. Wakasa *et al*., Phys. Rev. C **51**, R2871 (1995).
[46] Y. Sakemi *et al*., Phys. Rev. C **51**, 3162 (1995).
[47] A. Tamii *et al*., Phys. Lett. B **459**, 61 (1999).
[48] W. G. Love and M. A. Franey, Phys. Rev. C **24**, 1073 (1981).
[49] N. M. Hintz, A. M. Lallena, and A. Sethi, Phys. Rev. C **45**, 1098 (1992).